IET Microwaves, Antennas & Propagation

Research Article

Circularly polarised multiservice RFID antenna

ISSN 1751-8725
Received on 3rd May 2016
Revised on 2nd August 2016
Accepted on 16th August 2016
doi: 10.1049/iet-map.2016.0364
www.ietdl.org

Jayaram Kizhekke Pakkathillam ✉, *Malathi Kanagasabai*

Department of Electronics and Communication Engineering, College of Engineering, Guindy, Anna University, Chennai 600 025, India
✉ *E-mail: jayaramkarivellur@gmail.com*

Abstract: A multiservice radio-frequency identification (RFID) antenna with wideband axial ratio (AR) response around 2.4 GHz is presented in this study. This antenna offers dual band operation. The prototype follows a configuration constituting a driven element (radiator) and a parasitic element. The first band offers a voltage standing wave ratio (VSWR) bandwidth (3:1) of 183 MHz (0.85–1.04 GHz). The VSWR bandwidth (3:1) for the second band is 2.77 GHz (2–4.77 GHz). It also offers a 3 dB AR bandwidth of 1.1 GHz (2.1–3.2 GHz). The 2:1 VSWR bandwidth of 0.9 GHz (2.1–3 GHz) and cross-polarisation in the second band makes this antenna suitable for 2.4 GHz RFID reader applications. The other services supported by the proposed antenna include global system for mobile communication (0.88–0.96 GHz), long-term evolution (2.3–2.4 GHz), wireless fidelity (2.4–2.5 GHz), bluetooth low energy (2.4 GHz) and worldwide interoperability for microwave access (3.5 GHz). To extract the multiservice characteristics, it is necessary to integrate this antenna to a handheld computing platform. For assessing the performance in such a platform, the prototype is optimised and merged with a larger ground plane of size 170 mm × 130 mm and studied in the course of this study.

1 Introduction

Radio-frequency identification (RFID) systems allow tracking and identification of objects attached with RFID tags. One of the major requirements of these systems is infrastructure for reading and writing data from and to a database. Modern tablet computers are capable of processing data from multitude of sources. The versatility of these devises is increased with the help of multi-touch touchscreen display, accelerometers and many other sensing components. The integration of RFID readers and tablet computers is a new business model which will help faster tracking, processing and logging data to a database, as presented in [1] where wireless fidelity (Wi-Fi) is used as the medium for Internet. Ultra-high-frequency (UHF) RFID readers integrated to tablet devices are available commercially [2] where the Internet communication is established through wideband code division multiple access (WCDMA) service. This allows faster recording and processing of data wirelessly. It will be interesting if basic communication services: namely, global system for mobile communication (GSM) and worldwide interoperability for microwave access (Wi-MAX) are supported by these multiservice tablets. Compared with UHF RFID systems, 2.4 GHz RFID system detects tags more efficiently and swiftly in the presence of obstacles. Hence, a system having versatility of Internet access along with powerful RFID reading capability will result in efficient tracking and identification process for personal as well as industrial applications in the near future.

Initial developments in tablet antenna design can be found in [3]. In the literature, there are multiband antennas for tablet computers. References [4–14] deal with multiband and broadband antennas for wireless wide area network, long-term evolution (LTE) and other applications. These are efficient for the specified applications and are linearly polarised. A multiband mobile phone antenna with circularly polarised global positioning system operation is presented in [15]. Well-developed UHF RFID reader antennas are present in the literature [16]. The research on 2.4 GHz RFID readers requires some more attention. A linearly polarised microstrip patch antenna for 2.4 GHz RFID application is presented in [17]. Circular polarisation [18] is required for RFID applications in order to detect tags irrespective of its orientation. Reference [19] employs a 1×7 array of rectangular slot antenna for 2.4 GHz RFID application with narrow axial ratio bandwidth (ARBW). Reference [20] presents a dual band RFID reader antenna with broadband circular polarisation at 900 MHz and 2.4 GHz. Wideband circular polarisation will help in incorporating many communication services with higher degree of signal quality. References [21–25] deal with multiservice antennas for tablet application having only linearly polarised far-field.

A configuration of wideband radiator and a parasitic director element is presented in this paper. The combination of these two structures offers dual band operation as well as wideband circular polarisation. Novel aspects of the proposed prototype are achieving wide ARBW and a wide voltage standing wave ratio (VSWR) bandwidth (3:1) in the compact antenna element by deploying a combination of a wideband radiator and a y-shaped director element. The proposed prototype provides integration of multiple services: namely, RFID service, Wi-Fi, GSM, Bluetooth, Wi-MAX. The possible interference between RFID service and Wi-Fi/Bluetooth service can be avoided by employing required multiplexing scheme, spread spectrum coding [26] and internet protocol review techniques [27].

2 Multiservice antenna design

The multiservice antenna element and its dimension details are shown in Fig. 1. The detailed dimensions are $L = 48$ mm, $W = 29$ mm, $h = 1.6$ mm, $L_1 = 42$ mm, $w_1 = 26$ mm, $r = 3$ mm, $a = 31$ mm, $b = 13$ mm, $c = 6.5$ mm, $d = 18$ mm, $f = 0.8$ mm, $g = 3.5$ mm, $k = 12$ mm and $t = 0.8$ mm. The evolution of the multiservice antenna element is shown in Fig. 2.

2.1 Impedance characteristics

For antennas used in tablet computers and smartphone, the widely accepted and used VSWR level is 3:1. [4–10]. According to Saif

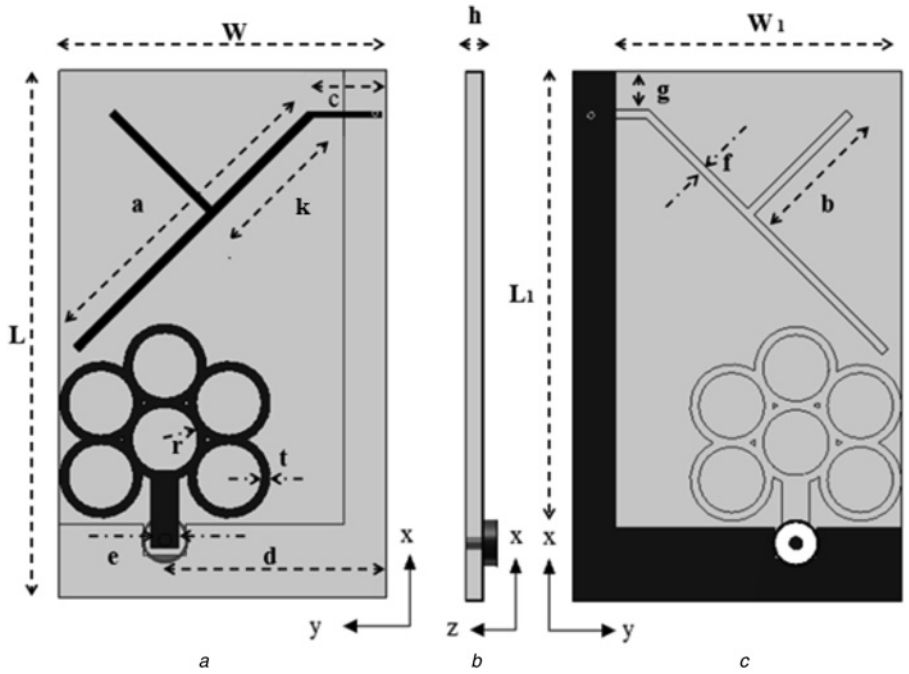

Fig. 1 *Schematic of the multiservice antenna*

a Front view
b Side view
c Rear view

and Alsmadi [28], the systems such as smartphones and tablet personal computers are low power devices and their radio requires less power. Higher-input RF power may even damage the radio. Hence, a VSWR level of 3:1 is suitable for the input RF power requirement. However, for the RFID operation, 2:1 VSWR bandwidth is calculated and is satisfactory for the application. The availability of attenuators will help in reducing the input RF power for various components in tablet part in 2.4 GHz band in case of a higher power input is received. Antenna 1 is a ring-shaped wideband radiator. Fig. 3*a* shows the reflection coefficient characteristics corresponding to the antennas 1, 2 and 3. It is observed from this figure that antenna 1 provides a wideband operation around 4.5 GHz. To bring down the frequency of operation, in antenna 2, three extra ring-shaped elements are added. This process shifts the centre frequency to 3 GHz. For further lowering of the operating range, antenna 3 is employed. This provides a wideband matching from 1.9 to 4 GHz.

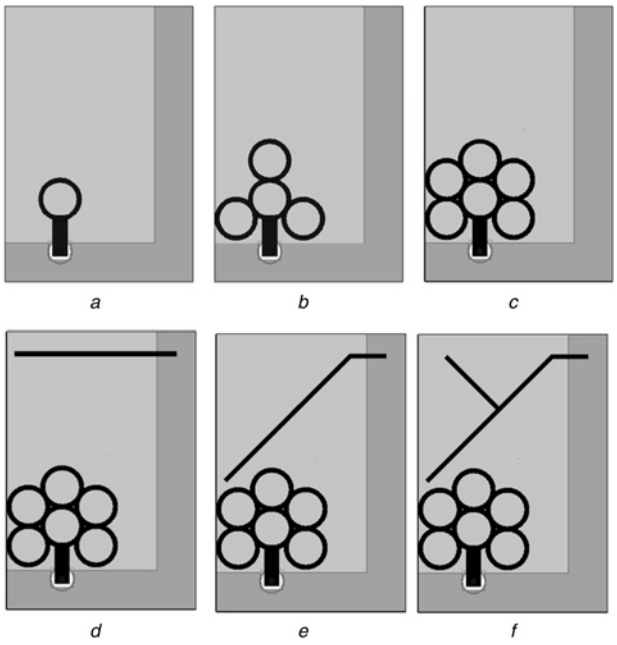

Fig. 2 *Evolution of the multiservice antenna*

a Antenna 1
b Antenna 2
c Antenna 3
d Antenna 4
e Antenna 5
f Antenna 6

Further from Fig. 3*b*, it can be observed that the antenna 4 consisting a straight parasitic director stub has the operating frequency range that starts from 1.3 GHz. When the stub is tilted 45° toward the radiator and the layout parameter 'a' is increased from 15 to 30 mm, an additional band at 900 MHz is obtained. This 45° tilted stub is extended close to radiator in order to increase coupling between the radiator and the parasitic element. Hence, the electrical distance has increased such that the resonance around 0.9 GHz can be brought on the antenna element. In the final prototype antenna 6, another stub (indicated by layout parameter 'b') is added. The angle between this second stub and 45° tilted stub is 90°. This provides a bandwidth of 170 MHz (17.4%) in the first band and 2.6 GHz (8.1%) in the second band.

The resonant modes for a conventional patch of length L, width and height h is given as follows as presented in [29]

$$f_{r(m,n,p)} = \frac{1}{2\pi\sqrt{\mu\varepsilon}}\sqrt{\left(\frac{m\pi}{L}\right)^2 + \left(\frac{n\pi}{h}\right)^2 + \left(\frac{p\pi}{w}\right)^2} \quad (1)$$

For the proposed radiator, the resonant modes are identified based on the principal layout parameter that contributes to various resonances. They are the effective perimeter of the radiator P_{er} and effective length of the director arm L_{ed}. On the basis of this configuration, the equation for overall resonant modes and for each mode are

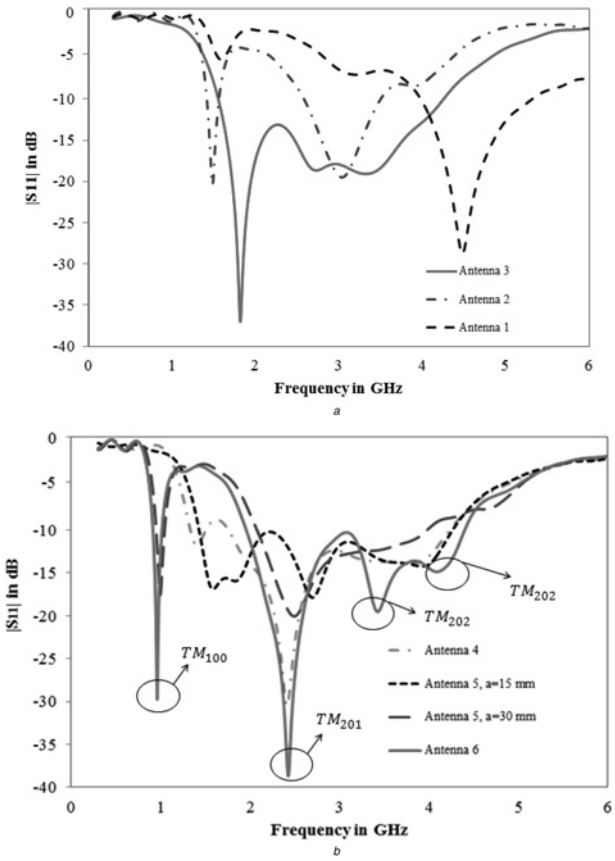

Fig. 3 *$|S_{11}|$ as a function of frequency for*

a For antennas 1, 2 and 3
b For antennas 4, 5 and 6

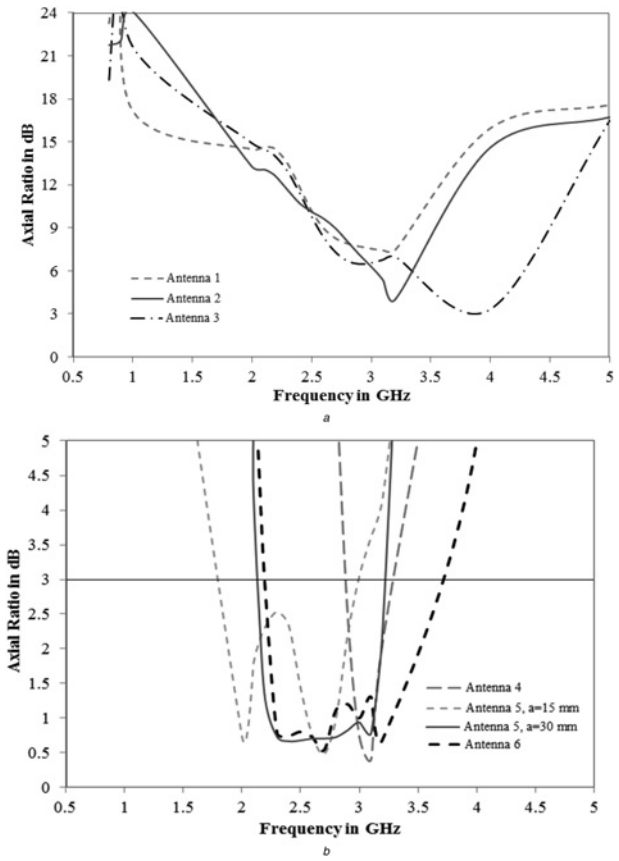

Fig. 4 *AR as a function of frequency*

a For antennas 1, 2 and 3
b For antennas 4, 5 and 6

identified and presented

$$f_{r(m,n,p)} = \frac{1}{2\pi\sqrt{\mu\varepsilon}}\sqrt{\left(\frac{m\pi}{P_{er}}\right)^2 + \left(\frac{n\pi}{h}\right)^2 + \left(\frac{p\pi}{L_{ed}}\right)^2} \quad (2)$$

$$P_{er} = 80\,\text{mm} \quad (3)$$

$$L_{ed1} = a + c = 37.5\,\text{mm}\ (\text{TM}_{202}\ \text{first resonance}) \quad (4)$$

$$L_{ed2} = 2 \times b + c = 32.5\,\text{mm}\ (\text{higher} - \text{order component}) \quad (5)$$

Closer occurrence of TM_{202} modes based on the layout parameter L_{ed1} and L_{ed2} leads to the formation of a wider band. The corresponding resonant modes obtained are indicated in Fig. 3*b*. Table 1 presents the details about resonant modes for the proposed prototype.

2.2 Radiation characteristics

Antennas 1, 2 and 3 are radiators, fed by vertical striplines. Hence, they have vertical polarisation as co-pol. To excite cross-polarisation (CP), the vertical and horizontal components of electric field (*E*-field) should have quadrature phase and equal amplitude. The near CP radiation in antennas 1, 2 and 3 are due to the slight offset feeding and ground plane protrusion. The AR response of these antenna systems are indicated in Fig. 4*a*.

Fig. 4*b* shows the AR response for antennas 4, 5 and 6. Antenna 4 has the straight parasitic element configuration which generates the horizontal component of *E*-field for a smaller range of frequencies. Hence, a narrow ARBW is observed. Antenna 5 has the angled parasitic element. When the length of the parasitic element is increased, wide ARBW is observed as the structure serves quadrature phase for a larger set of frequencies. Again in antenna 6, the two stubs of the *Y*-shaped director element provide a resultant horizontal component of *E*-field, which is equal to the

Table 1 Resonant modes of the proposed antenna

Mode	Equation	P_{er}, mm	L_{ed}	Frequency in GHz (calculated)	Frequency in GHz (simulated)
TM_{100}	$f_{r(1,0,0)} = \frac{1}{2\sqrt{\mu\varepsilon}}\sqrt{\left(\frac{1}{P_{er}}\right)^2}$	80	NA	0.9041	0.912
TM_{201}	$f_{r(2,0,1)} = \frac{1}{2\sqrt{\mu\varepsilon}}\sqrt{\left(\frac{2}{P_{er}}\right)^2 + \left(\frac{1}{L_{ed}}\right)^2}$	80	32.5 mm	2.4215	2.375
TM_{202}	$f_{r(2,0,2)} = \frac{1}{\sqrt{\mu\varepsilon}}\sqrt{\left(\frac{1}{P_{er}}\right)^2 + \left(\frac{1}{L_{ed}}\right)^2}$	80	37.5 mm	3.6923	3.498
TM_{202}	$f_{r(2,0,2)} = \frac{1}{\sqrt{\mu\varepsilon}}\sqrt{\left(\frac{1}{P_{r}}\right)^2 + \left(\frac{1}{L_{d}}\right)^2}$	80	32.5 mm	4.5123	4.295

IET Microw. Antennas Propag., 2017, Vol. 11, Iss. 2, pp. 232–239

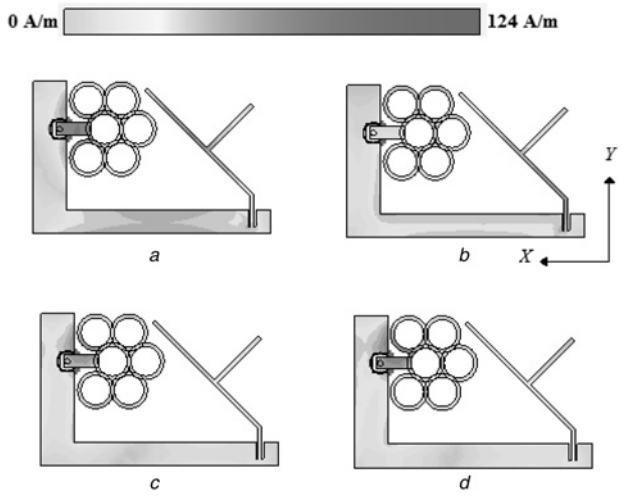

Fig. 5 *Current flow over the antenna plane*

a 0.9 GHz
b 2.4 GHz (0°)
c 2.4 GHz (90°)
d 3.6 GHz

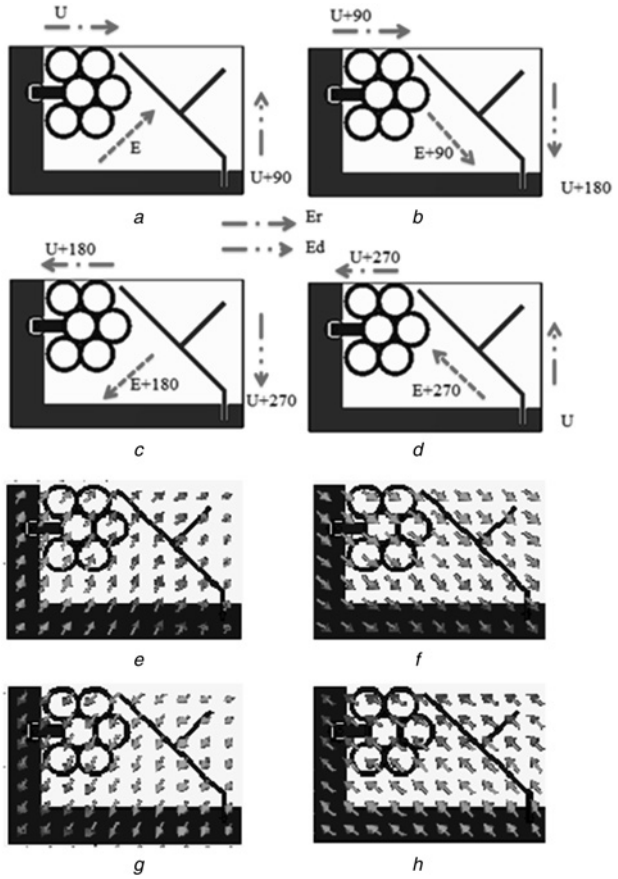

Fig. 6 *E-field over the antenna plane at arbitrary input phase angles*

a $U°$
b $U + 90°$
c $U + 180°$
d $U + 270°$
E-field at
e 135°
f 225°
g 315°
h 45°

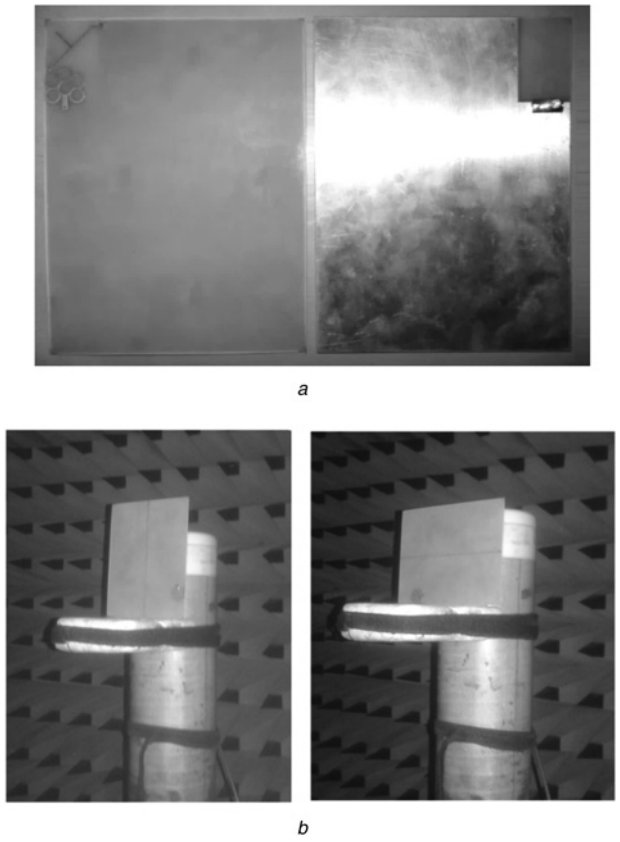

Fig. 7 *Fabricated prototype and measurement*

a Obverse and reverse views of antenna element integrated to a large ground plane
b Antenna under test, both in portrait and landscape orientations

vertical component of *E*-field generated by the wideband radiator with phase quadrature over a wide-frequency range.

3 Principle of operation

3.1 Current flow over XY-plane

The current flow over the antenna plane for different operating frequencies has been presented in Fig. 5. From the current flow diagram, it can be identified that the coupling between the radiator and director is occurring at 900 MHz and is the reason for the generation of lower band. This is because the current coupled through the parasitic element travels through parasitic element of larger electrical length. This trend is not followed by the higher frequency as the wideband radiator is resonating for the second

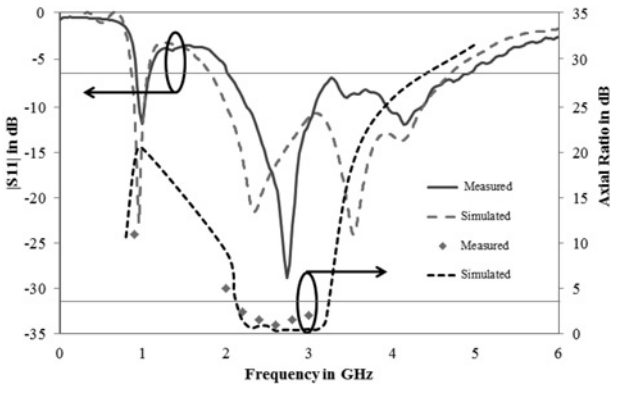

Fig. 8 *Simulated and measured $|s_{11}|$ and AR as a function of frequency for the antenna element integrated to a large ground plane*

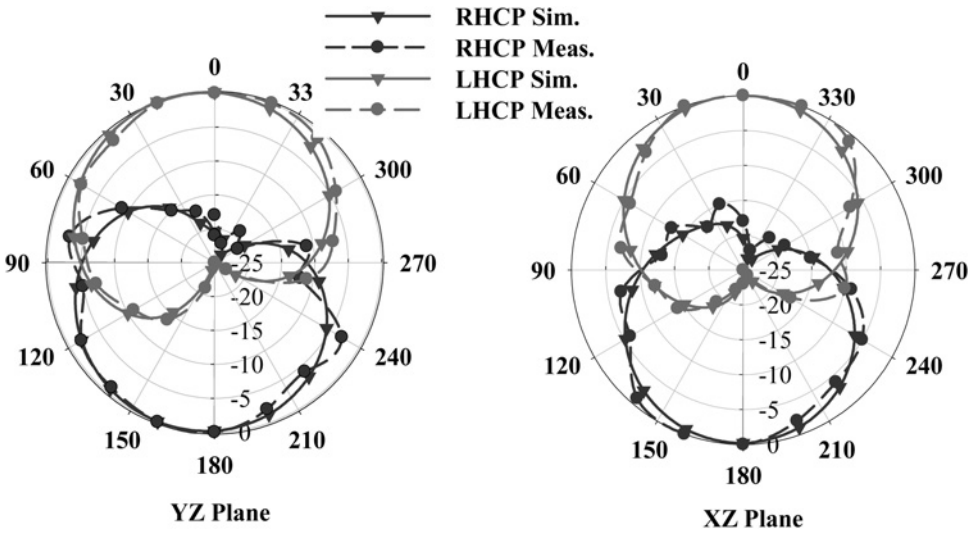

Fig. 9 *Simulated and measured CP patterns at 2.4 GHz*

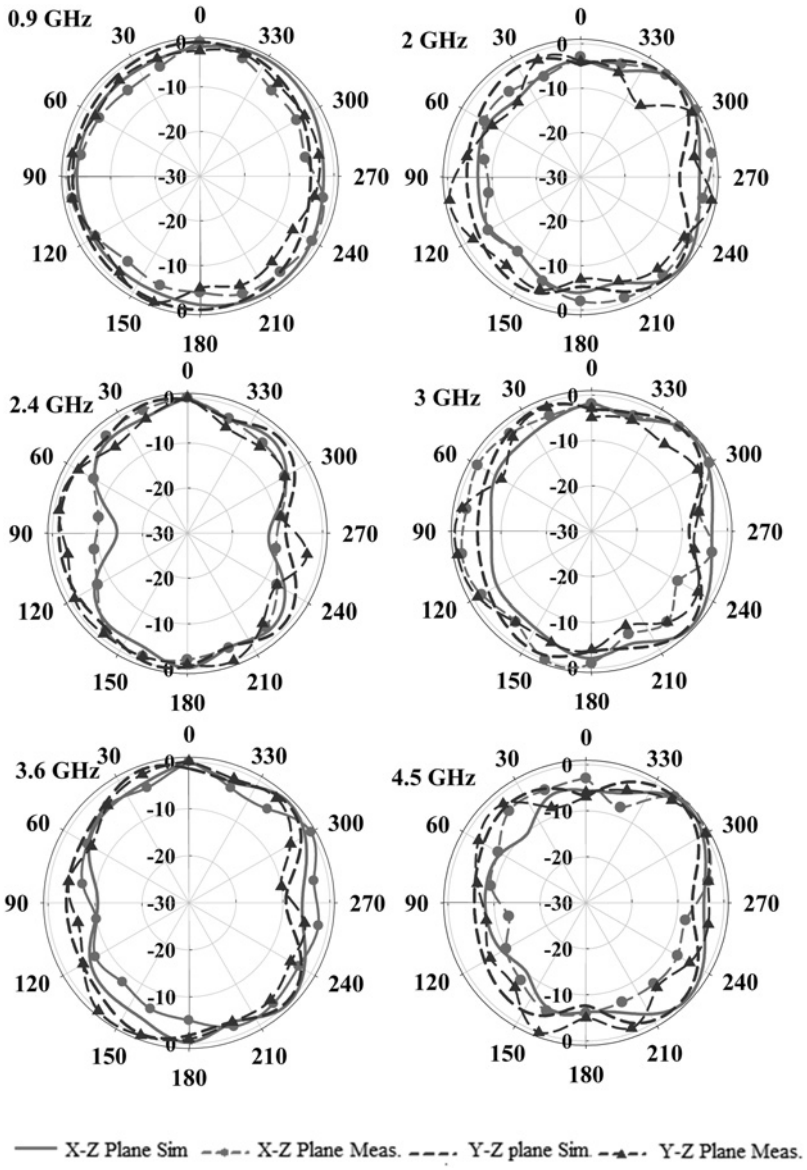

Fig. 10 *Simulated and measured radiation patterns*

IET Microw. Antennas Propag., 2017, Vol. 11, Iss. 2, pp. 232–239

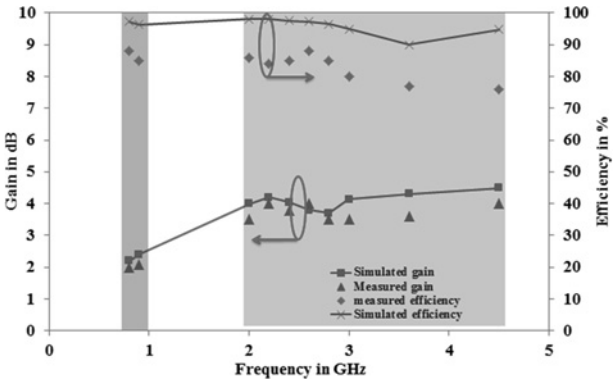

Fig. 11 *Gain and efficiency (simulated and measured) as a function of frequency*

band. The CP in the 2.4 GHz band is generated through the alternate excitation of the radiator and the parasitic element as shown in Figs. 5*b* and *c*. Here at the current phase angle equals 0°, the parasitic element gets excited and results in the orientation of field in the direction 180° opposite to the current traversing path (here along *Y*-axis). When the phase angle value is 90°, the wideband radiator becomes excited and the *E*-field orientation becomes aligned with the *X*-axis.

3.2 E-field distribution

The *E*-field over *xy*-plane of the antenna element is illustrated in Fig. 6. Generalised explanation for the *E*-field generation is given by investigating the association of *E*-field components (Er due to radiator and Ed due to director) over the *xy*-plane, starting from an arbitrary phase angle '*U*' as in Fig. 6*a*. The resultant *E*-field is given as *E*. In Fig. 6*b*, after an input phase change of 90°, Er is in the same direction as that of Er in Fig. 6*a* but the direction of Ed gets changed due to the extra 90° separation between radiator and director elements in the proposed design. Hence, resultant *E*-field is rotated to $E+90°$ position. In Fig. 6*c*, the direction of Er gets reversed as an input current phase value of $U+180°$ is present. No reversal in Ed component as only 90° is added to it and total phase is $U+270°$. The resultant *E*-field rotates to $E+180°$ position. In Fig. 6*d*, Er is in the same orientation as of the previous state. Ed component reverses the direction as the condition $U+270°+90°$ has occurred, which is same as *U*. This results in the rotation of *E*-field *E* to $E+270°$ position. This rotation of the *E*-field results in the circularly polarised radiation from the proposed antenna.

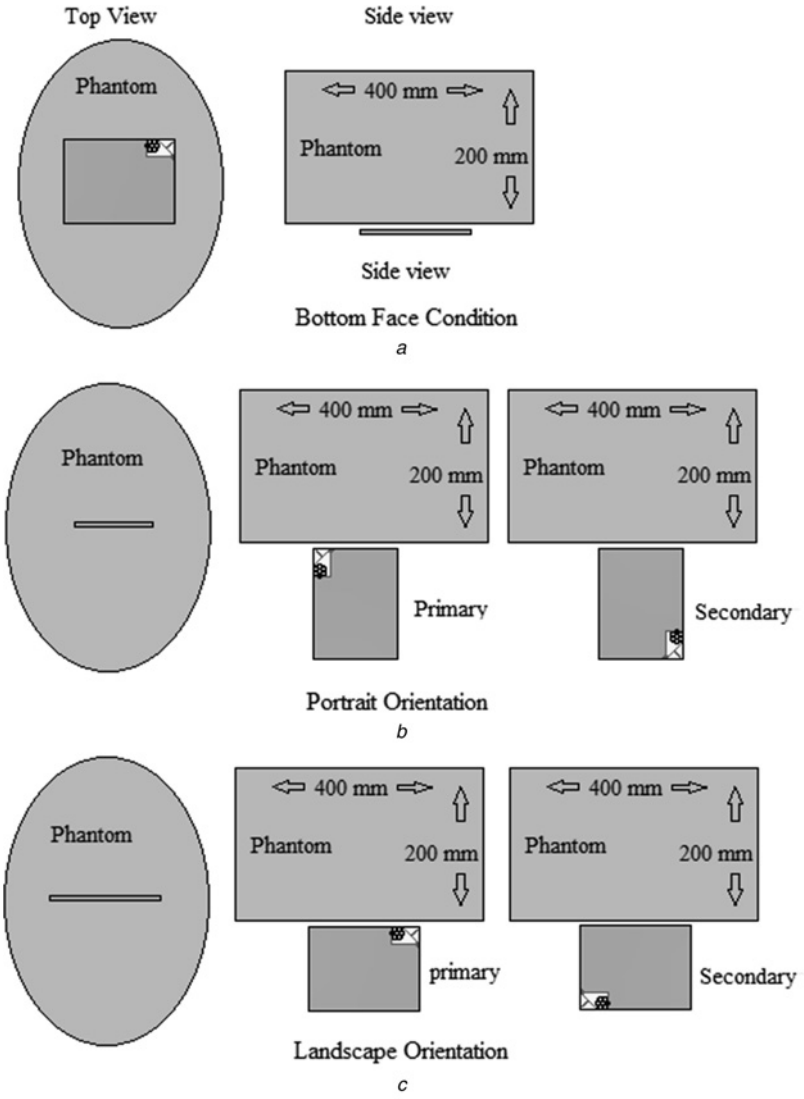

Fig. 12 *SAR analysis conditions*

a Bottom face
b Portrait
c Landscape

Table 2 SAR analysis for the proposed antenna

Frequency	900 MHz	2.2 GHz	2.4 GHz	3.6 GHz
power, W	0.125	0.125	0.125	0.125
bottom face condition	1.12	1.32	0.97	1.03
primary landscape orientation	1.24	1.15	0.79	0.98
primary portrait orientation	1.36	1.06	0.94	0.93
secondary landscape orientation	0.029	0.032	0.05	0.012
secondary portrait orientation	0.022	0.020	0.032	0.018

4 Fabrication, measurement and performance analyses

The antenna element is optimised and integrated to a ground plane of size 170 × 130 mm for utilising the multiservice capabilities in a handheld tablet computer platform. The radiator with a parasitic element configuration is fabricated on flame retardant–grade 4 substrate of 1.6 mm thickness with dielectric constant (ε_r) = 4.4 and dielectric loss tangent (tan δ) = 0.025. The obverse and reverse views of the antenna element integrated to the larger ground plane and measurement scenario are shown in Fig. 7. The reflection coefficient measurement is carried out using an Agilent E5070A two-port RF network analyser.

4.1 Impedance and radiation performance

Fig. 8 shows the simulated and measured results for the antenna integrated with a large ground plane. The lower band (measured) is from 857 MHz to 1.04 GHz (183 MHz at VSWR ≤ 3). A fractional bandwidth of 20.3% is achieved in this band at the centre frequency of the band, 948 MHz. The measured upper band is from 2 to 4.77 GHz (2.77 GHz at VSWR ≤ 3). The fractional bandwidth corresponding to second band is 8.1% at the centre frequency of the band, 3.38 MHz. Fig. 9 shows the simulated and measured CP pattern (left hand circular polarisation and right hand circular polarisation) for the antenna at 2.4 GHz with a large ground plane. Fig. 10 shows the simulated and measured radiation patterns for different frequency of operation.

The gain and efficiency plot for the proposed antenna is shown in Fig. 11. A maximum gain of 4.15 dB is obtained in the operating band. The operating bandwidth is covered by the 3 dB gain-bandwidth reference line. Similar trend is followed by the measured gain. A maximum measured efficiency of 88% is reported at 2.6 GHz. The measured efficiency varies between 88 and 76% in the operating band.

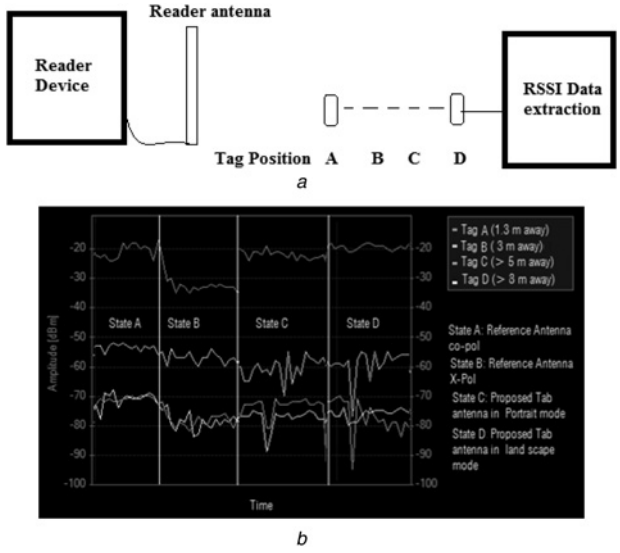

Fig. 13 *Read range measurement*
a Set up schematic
b RSSI data

4.2 Specific absorption rate (SAR) analysis

The SAR is the rate at which the electromagnetic energy is absorbed by human body when exposed to the same. It depends on the electrical conductivity of the sample tissue, the root-mean-square value of generated *E*-field by the device under test, density and the volume of the tissue sample.

The five conditions at which the SAR study carried out are bottom face condition, primary landscape orientations, secondary landscape orientation, primary portrait orientation and secondary portrait orientation. For the evaluation of SAR for this particular antenna, a phantom of $\varepsilon_r = 53$ [30] is employed. The distance of separation between the antenna and phantom in the bottom face condition is 8 mm. In portrait and landscape conditions, the separation between phantom and antenna is kept as 6 mm. The dimension details of the phantom and different orientation of the antenna for SAR analysis are given in Fig. 12. As shown in this figure, the secondary landscape and portrait orientations keep the antenna around 100 mm away from the phantom. Hence, the obtained SAR values are negligible compared with the SAR limit of 1.6 W/kg (1 g tissue). In bottom face condition, the maximum SAR obtained is 1.32 W/kg at 2.2 GHz. The primary landscape orientation results in a maximum SAR of 1.24 W/kg at 900 MHz. Primary portrait orientation records a maximum SAR of 1.36 W/kg at 900 MHz. The SAR values at different frequencies have been presented in Table 2. SAR is calculated for a reference power of 0.125 W and the averaging method used is IEEE C95.3. SAR values in the analysed conditions indicate satisfactory performance for the proposed antenna on 1 g tissue standard.

4.3 Read range measurements

The read range measurement is carried out for the proposed antenna (Fig. 13*a*). The reference technology for the measurement based on received signal strength indicator (RSSI) is given in [31]. First, a linearly polarised reference antenna of 4 dB gain is connected to a 2.4 GHz RF transceiver. A receiver antenna with 2 dB gain is connected to a system providing the RSSI against time response. This antenna is placed at different tag antenna positions (tags A, B, C and D). Tag position B is 3 m away from the reader. Tag positions C and D are 6 and 8 m, respectively. The distance between tag position A and reader is adjusted such that the coupling between them is maintained around −20 dBm. This gives the read distance. Fig. 13*b* shows the RSSI response for this system. During state A, tag and reader (reference) antennas are in same polarisation. When the polarisation of the reference antenna is switched (state B), the tag–reader coupling is getting deteriorated. State C indicates the coupling between tag and the proposed reader antenna operating in portrait mode. When the orientation is switched to landscape mode as in state D, the coupling is not affected owing to the circular polarisation property of the proposed reader antenna. The maximum obtained read distance for the proposed antenna for the above-mentioned condition is 1.3 m.

5 Conclusion

A compact multiservice antenna with wideband circular polarisation has been presented for integrating RFID service with tablet computers. The prototype offers dual band operation with 20% bandwidth in first band as well as 8.1% in second band. The ARBW of 4% is obtained at the second band. The antenna is fabricated and the performance is validated through measurement. The RFID service offers a read range of 1.3 m. The SAR analysis shows satisfactory performance. The communication services: namely, GSM, LTE, WCDMA, Wi-Fi and bluetooth low energy are

supported by this particular antenna. Hence the tracking, identification and communication entities can be integrated into a single platform.

6 References

1 HABEY, USA. Intel Atom Z510 TPC-6507 Rugged 7' Tablet PC. Available at http://www.habeyusa.com/wp-content/uploads/2012/12/TPC-6507.pdf
2 CILICO, USA. UHF RFID Reader PDA. Available at http://www.cilico.us/products/android-uhf-rfid-tablet.html
3 Huang, C.-F., Chiu, C.-H.: 'A WLAN-used helical antenna fully integrated with the PCMCIA carrier', *IEEE Trans. Antennas Propag.*, 2005, **53**, (12), pp. 4164–4168
4 Ban, Y.-L., Sun, S.-C., Li, P.-P., *et al.*: 'Compact eight-band frequency reconfigurable antenna for LTE/WWAN tablet computer applications', *IEEE Trans. Antennas Propag.*, 2014, **62**, (1), pp. 471–475
5 Lu, J.-H., Tsai, F.-C.: 'Planar internal LTE/WWAN monopole antenna for tablet computer application', *IEEE Trans. Antennas Propag.*, 2013, **61**, (8), pp. 4358–4363
6 Shen, S.-M., Chen, I.-F., Peng, C.-M., *et al.*: 'Printed asymmetric dual-dipole antenna for tablet PC applications', *IEEE Antennas Wirel. Propag. Lett.*, 2013, **12**, pp. 1003–1005
7 Chou, J.-H., Chang, J.-F., Lin, D.-B., *et al.*: 'A compact loop-slot mode combination antenna for ultra-thin tablet computer with metallic bottom cover', *IEEE Antennas Wirel. Propag. Lett.*, 2014, **13**, pp. 746–749
8 Lu, J.-H., Lin, Z.-W.: 'Planar compact LTE/WWAN monopole antenna for tablet computer application', *IEEE Antennas Wirel. Propag. Lett.*, 2013, **12**, pp. 147–150
9 Chen, W.-S., Jhang, W.-C.: 'A planar WWAN/LTE antenna for portable devices', *IEEE Antennas Wirel. Propag. Lett.*, 2013, **12**, pp. 19–22
10 Lu, J.-H., Wang, Y.-S.: 'Planar small-size eight-band LTE/WWAN monopole antenna for tablet computers', *IEEE Trans. Antennas Propag.*, 2014, **62**, (8), pp. 4372–4377
11 Alsath, M.G.N., Kanagasabai, M.: 'Planar pentaband antenna for vehicular communication application', *IEEE Antennas Wirel. Propag. Lett.*, 2014, **13**, pp. 110–113
12 Ameelia Roseline, A., Kanagasabai, M.: 'Compact dual-band patch antenna using spiral shaped electromagnetic bandgap structures for high speed wireless networks', *AEU – Int. J. Electron. Commun.*, 2012, **66**, (12), pp. 963–968
13 Natarajan, R., George, J., Kanagasabai, M., *et al.*: 'A compact antipodal Vivaldi antenna for UWB applications', *IEEE Antennas Wirel. Propag. Lett.*, 2015, **14**, pp. 1557–1560
14 Sivasamy, R., Kanagasabai, M., Baisakhiya, S., *et al.*: 'A novel shield for GSM 1800 MHz band using frequency selective surface', *Prog. Electromagn. Res. Lett.*, 2013, **38**, pp. 193–199
15 Liang, Z., Li, Y., Long, Y.: 'Multiband monopole mobile phone antenna with circular polarization for GNSS application', *IEEE Trans. Antennas Propag.*, 2014, **62**, (4), pp. 1910–1917
16 Raviteja, C., Varadhan, C., Kanagasabai, M., *et al.*: 'A fractal-based circularly polarized UHF RFID reader antenna', *IEEE Antennas Wirel. Propag. Lett.*, 2014, **13**, pp. 499–503
17 Rahman, M.A., Shaikat, A., Iqbal, I.S., *et al.*: 'Microstrip patch antenna design and performance analysis for RFID applications at ISM band (2.45 GHz)'. 2013 Int. Conf. on Advances in Electrical Engineering (ICAEE), 19–21 December 2013, pp. 305–308
18 Kizhekke Pakkathillam, J., Kanagasabai, M.: 'Circularly polarized broadband antenna deploying fractal slot geometry', *IEEE Antennas Wirel. Propag. Lett.*, 2015, **14**, pp. 1286–1289
19 Huang, T.-J., Lin, S.-C., Hsu, H.-T.: '1-by-7 circularly-polarized shaped-beam antenna array for radio frequency identification (RFID) reader applications at 2.4 GHz'. 2013 IEEE Antennas and Propagation Society Int. Symp. (APSURSI), 7–13 July 2013, pp. 1736–1737
20 Jung, Y.-K., Lee, B.: 'Dual-band circularly polarized microstrip RFID reader antenna using metamaterial branch-line coupler', *IEEE Trans. Antennas Propag.*, 2012, **60**, (2), pp. 786–791
21 Wong, K.L., Wei, W.J., Chou, L.C.: 'WWAN/LTE printed loop tablet computer antenna and its body SAR analysis', *Microw. Opt. Technol. Lett.*, 2011, **53**, pp. 2912–2919
22 Chang, S.H., Liao, W.J.: 'A broadband LTE/WWAN antenna design for tablet PC', *IEEE Trans. Antennas Propag.*, 2012, **60**, pp. 4354–4359
23 Liu, H.W., Chiang, C.M., Yang, C.F.: 'Planar monopole antenna with two coupled strips for internal eight-band LTE/WWAN laptop computer application', *Prog. Electromagn. Res. C*, 2012, **29**, pp. 123–133
24 Ibra, D., Aliou, D., Sidi, M.F., *et al.*: 'Compact dual-band monopole antenna for LTE mobile phones'. Proc. Loughborough Antennas and Propagation Conf., 2010, pp. 593–596
25 Wong, K.-L., Lin, W.-J.: 'WWAN/LTE printed slot antenna for tablet computer application', *Microw. Opt. Technol. Lett.*, 2012, **54**, pp. 44–49, doi: 10.1002/mop.26509
26 Wei, J., Ma, Y.: 'Interference analysis of microwave RFID and 802.11b WLAN'. 2007 Int. Conf. on Wireless Communications, Networking and Mobile Computing, Shanghai, 2007, pp. 2062–2065
27 RFID – the risk of interference by Core RFID. Available at http://www.corerfid.com/rfid-technology/technology-issues/rfid-and-interference/
28 Saif, K., Alsmadi, N.: 'Mobile phone antenna design', 2015. Available at http://www.bth.diva-portal.org/smash/record.jsf?pid=diva2:840332
29 Ismail, M.K.H., Esa, M.: 'Resonant modes configurations for rectangular antenna based on cavity model'. The Ninth Asia-Pacific Conf. on Communications, 2003. APCC 2003, 2003, vol. 3, pp. 954–958
30 Clibration procedure for dipole validation kits above 700 MHz. Available at: https://www.fccid.io/pdf.php?id=1847617
31 Luh, Y., Liu, Y.: 'Measurement of effective reading distance of UHF RFID passive tags', *Mod. Mech. Eng.*, 2013, **3**, (3), pp. 115–120, doi: 10.4236/mme.2013.33016